A tool for deciphering the redox potential ranking of organic compounds: the case study of biomass extracted quinones for sustainable energy

Fanny Lambert, Yann Danten, Carlo Gatti, Christine Frayret

PCCP
Physical Chemistry Chemical Physics

Accepted Manuscript

This article can be cited before page numbers have been issued, to do this please use: F. Lambert, Y. Danten, C. Gatti and C. Frayret, *Phys. Chem. Chem. Phys.*, 2020, DOI: 10.1039/D0CP02045A.

This is an Accepted Manuscript, which has been through the Royal Society of Chemistry peer review process and has been accepted for publication.

Accepted Manuscripts are published online shortly after acceptance, before technical editing, formatting and proof reading. Using this free service, authors can make their results available to the community, in citable form, before we publish the edited article. We will replace this Accepted Manuscript with the edited and formatted Advance Article as soon as it is available.

You can find more information about Accepted Manuscripts in the Information for Authors.

Please note that technical editing may introduce minor changes to the text and/or graphics, which may alter content. The journal's standard Terms & Conditions and the Ethical guidelines still apply. In no event shall the Royal Society of Chemistry be held responsible for any errors or omissions in this Accepted Manuscript or any consequences arising from the use of any information it contains.

View Article Online
DOI: 10.1039/D0CP02045A

ARTICLE

A tool for deciphering the redox potential ranking of organic compounds: the case study of biomass extracted quinones for sustainable energy

Received 00th January 20xx,
Accepted 00th January 20xx

DOI: 10.1039/x0xx00000x

Fanny Lambert,[a] Yann Danten [b] and Carlo Gatti [c] and Christine Frayret,*[a]

Carbonyl compounds have emerged as promising organic electrodes for sustainable energy storage. Accelerating the process of performant materials discovery relies on the possibility of developing methodologies to enable the scan of various sets of candidates. The genesis of such educated guess strategy has to be privileged to reduce the search space of experiments, accelerate this research area and contribute to the sustainable effort. To address this challenge, we built a quantitative structure-activity relationship to unveil the origin of the redox potential magnitude as a function of both structural features and complexation effects. The potential of this prediction model is demonstrated on various *ortho*-quinones directly deriving from naturally occurring catechols. Beyond the modulation provided by substituent change, the possibility of calling to various kinds of alkaline(-earth)-ion electrochemistry is examined thoroughly. The power of partitioning the total molecular energy into additive atomic group contributions is highlighted and the built-up of this robust strategy enables a guidance towards rational selection of most suited compound/metal-ion couples. An upshift/downshift of the redox potential by switching from Li to Mg/Na is revealed, while the identification of the relative role played by the various components of the systems as well as electrostatic interactions is clearly identified. These results, particularly the evidence of different substituent effects on the single/double reduction potentials and as a function of type of electrochemistry (Li/Na/Mg), have important implications for designing new electroactive compounds with tailored redox properties.

1. Introduction

Among other great inventions, electricity generation has transformed the world. Nowadays, humanity and our modern life cannot be disentangled from the needs to pay attention to the rising worldwide consumption of energy. Being part of our daily life, various kinds of habits including lighting through electricity, the use of electrical and electronic devices, calling to stationary energy storage systems as well as electric transportation therefore poses the challenge of balancing electricity demand and power supply over time. In the energy landscape, Li-ion batteries (LIBs) corresponding to a specific kind of chemically storing energy based on electrochemistry principles have emerged as viable for several applications. On the other hand, if electric vehicles are considered as cleaner alternatives to conventional transportation with much less greenhouse gas emission, embarked LIBs (like other kinds of batteries) will be forced to face a new deal with directives and rules imposing to fulfil new requirements especially in terms of recycling (battery directive 2006/66/EC: "The primary objective of this Directive is to minimize the negative impact of batteries and accumulators and waste batteries and accumulators on the environment […]"). In the field of batteries, one way towards ever-smaller, more powerful and portable electronic devices, may rely on a smart fit between new innovative materials and advanced technologies. Electrical vehicles constitute in particular one of the markets directly concerned by the future of LIBs for which reaching high-performance and inexpensive electricity storage is of utmost

[a] Laboratoire de Réactivité et Chimie des Solides (LRCS), UMR CNRS 7314, Université de Picardie Jules Verne, Hub de l'Energie, 15 Rue Baudelocque, 80000 Amiens Cedex France. Réseau sur le Stockage Electrochimique de l'Energie (RS2E), FR CNRS 3459, France. *E-mail: christine.frayret@u-picardie.fr
[b] Institut des Sciences Moléculaires, UMR CNRS 5255, 351 Cours de la Libération, 33405 Talence, France.
[c] CNR SCITEC, CNR Istituto di Scienze e Tecnologie Chimiche "Giulio Natta", Sede Via C. Golgi, 19,20133 Milano, Italy.
Electronic Supplementary Information (ESI) available: [details of any supplementary information available should be included here]. See DOI: 10.1039/x0xx00000x

View Article Online
DOI: 10.1039/D0CP02045A

relevance. Beyond endeavours to discover chemistries that would lead to cheaper, denser, lighter and more powerful LIBs, a few new battery technologies with transformative potential are envisioned for the future. Beyond the possibility to switch to Sodium-Ion Batteries (SIBs), the ways to look forward in years to come could indeed be linked to the advent of new devices and different approaches that go beyond traditional Li-ion technology. In particular, research has recently focused on the following promising avenues: the solid-state batteries using solid electrolytes, the Li-S, Na-S, Li-O batteries, which replace the intercalation phenomenon at the electrodes with high energy chemical reactions and the multivalent devices, which substitute the monovalent Li^+ ions with di- or tri-valent ions: Mg^{2+}, Al^{3+}, … and potentially double or triple the stored and released capacity. One should also add to this list, the redox flow-battery technology, which replaces solid electrodes with liquid solutions, and especially that based on high-voltage organic electrolytes and polymer active materials. In parallel and within the same context of growing need to store increasing quantities of sustainably generated electrical energy, organic materials as potential new kinds of electrodes for LIBs have attracted intensive research interest. Their pros include especially structural diversity, low cost, and redox potential tunability. Being made of naturally abundant elements (*e.g. C*, *H*, *O*, *N*, *S*), they lead to non-toxic materials, characterized by easier recycling and potential extraction from biomass. Since batteries are evolving to integrate new form factors, becoming ultra-thin as well as rollable, stretchable, etc, the possibility of generating flexible organic films or a variety of device architectures with this new kind of electrode is beneficial. In this new area, applications of quinone-functionalized materials to energy harvesting and storage is nowadays recognized[1,2]. By playing a vital role in important biological processes, quinones are ubiquitous in nature (see *e.g.*[3]). They involve electrochemical reactions for energy transduction and storage, including respiration and photosynthesis. A subset of important quinones corresponding to heterocyclic derivatives encompasses the indolequinone natural product mitomycin C (MMC)[4,5,6,7]. Catechols, which are easily transformed into quinones, are characterized by a strong binding affinity for various multivalent metal ions, this feature being useful in the field of a multivalent ion-energy storage as demonstrated for instance by Kim *et al.*[8], who proved the two-electron oxidation of catechol to quinone with a reversible extraction of Mg^{2+} cations during charging, and the reverse reaction of Mg^{2+} ions insertion during discharging. Independently, it was proved advantageous, with the purpose of rising the redox voltage, to introduce Mg^{2+} simply as a spectator cation in *p*-DHT (thus generating the $Mg(Li_2)$-p-DHT·H_2O system)[9].

In the search for improved organic electrodes, molecular DFT computations provide a first indication on the compounds capabilities prior to any experimental characterization of the crystalline organic phases and may thus facilitate the design of most promising redox-active systems by furthermore contributing to the efforts of restricting the time, cost and environmental footprint associated to the search of such advanced organic electrodes. Beyond anterior considerations on global molecular indicators able to account for redox properties (see *e.g.* the work of Beheshti *et al.* [10]), we already elucidated various structure-property relationships and proposed new potential candidates. We first quantitatively estimated the incidence of substituent effects on the *para*-benzoquinone redox activity, and demonstrated that it considerably enlarges the redox potential window and therefore constitutes one the most used way to tune the intrinsic redox property of a backbone[11]. Thanks to such kinds of screening, withdrawing groups were recognized to induce an increase in redox potential whereas

View Article Online
DOI: 10.1039/D0CP02045A

electron donating groups were characterized by the reverse trend. We furthermore demonstrated that electron withdrawing groups tend to stabilize reduced forms, while electron donating groups stabilize the initial forms. A deep insight into the mechanisms underlying the division of quinoneazine derivatives (quinoid-like structures separated through a bridge between two six-membered rings (6MRs), each one bearing only one carbonyl group) into low- and high-voltage systems was achieved this way, by evidencing in particular the indirect incidence of the bridge chemical bonding nature[12]. By discovering through these studies that N substitution in these quinoid-like rings could increase the voltage by a non-negligible amount, we then focused on pentalenedione derivatives and evaluated the joined incidence of isomerism and N single/double substitution for CH in the rings of these systems, proving that combined actions enable large modulation (of ~1.4V) in the redox voltage (the shifting towards higher values linked to N substitution being equal to 0.3-0.4 V in the case of single replacement and as high as 0.8-1.0 V for double substitutions)[13]. A similar approach was employed to elucidate the redox potential ranking of naphtho-, biphenyl- and biphenylenequinone isomers[14].

While Density Functional Theory (DFT) computations have been largely employed on quinonic compounds or derivatives in the past (see *e.g.* [15,16,17,18,19,20]), deep understanding of redox activity for a few substituted benzoquinones directly originating from nature, is still lacking in the context of energy storage. Indeed, such systems represent a far more advantageous alternative relative to naphthoquinones or anthraquinones as far as capacity is concerned. Otherwise, machine learning and high-throughput calling solely to DFT calculations, which are currently largely deployed to discover the most promising candidates for organic and redox-flow batteries do not give directly access to a specific rationalization of the predicted electrochemical features. More specifically, whereas the possibility of tuning the redox potentials through substitutions involving functional groups (in addition to isomerism effect, etc) is at the forefront of current experimental and theoretical investigations (see *e.g.* [15,16,21,22]), a very detailed analysis of the relative role played by the backbone, the redox centres, the functional group nature, and the type of electrochemistry (monovalent/multivalent), is in particular still missing.

Despite a large number of studies, there are thus questions with particular relevance for energy storage that remain to be answered regarding the search for optimal compounds. In particular, questions such as “Is there a tool able to identify the preferential sites in the neighbourhood of the molecular system that electrostatically binds to the metal?", “Is it possible to account for substituent effects in a set of *ortho*-quinone (*o*-quinone) systems?”, “What is the relative effect of the various pieces of the molecule in the extent of the redox potential ?”, “What is the differentiation of substituent effects on the 1 e- *vs.* 2 e- reduction potentials ?", “How can we rationalize the redox voltage change as a function of the type of electrochemistry (*i.e.* Li/Na/Mg etc) ?", remain to be answered. We address these issues in a systematic manner on the selected set of naturally occurring quinones and interpret our predicted features in light of the above-mentioned strategy.

At variance with the standard attempts to search for direct relationships between molecular redox potentials and frontier orbitals (*i.e.* the highest occupied molecular orbital, HOMO, or the lowest unoccupied molecular orbital, LUMO)[23,24,25,26,27,28,29], or to empirically relating them to the substituent effects through the Hammett-Zuman model[30], it is highly desirable to define a quantum chemical approach able to account for the electrochemical features while being at the same time fully independent of the nature of the

View Article Online
DOI: 10.1039/D0CP02045A

studied systems. By assuming that the Koopmans' theorem keeps its validity within the Kohn Sham (KS) model, linear relationships between the redox potentials gained from DFT calculations and frontier orbitals values have been searched for. However, these relationships show in certain cases some degree of discrepancy with respect to the linearity. Besides, it is normally not possible to retrieve electron affinity through KS LUMO for instance since its physical meaning is related to vertical excitation. Likewise, despite a certain ability in predicting the redox potentials for quinone compounds, the Hammett-Zuman approach cannot be considered as a universal methodology since it depends on empirical relationships that sometimes do not work in a general way. For instance, it has been proven that applying such model requires to group the quinone compounds into arbitrary families (*i.e.* benzoquinone, naphthoquinone, and anthraquinone) to be efficient[31]. Similarly, deviations from a linear scaling relationship were evidenced for quinones that feature intramolecular hydrogen bonding in the hydroquinone, halogen substituents, charged substituents, and/or sterically bulky substituents[30]30. Apart from these misconceptions or empirical predictions, the quest for actual structure-property relationships was examined based notably on the consideration of electrophilicity[32], electron delocalization or Clar theory[29], or Fukui functions[31]. Our global methodology lies in this class of approaches, which are aimed at examining features that stem directly from molecular properties. In view of rationalizing molecular redox potential trends and demonstrating the ability to use this strategy as an educated guess for reaching tailored redox active materials, we used the powerful arsenal described in Figure 1 (described hereafter). This approach has been applied to various *o*-quinone compounds, which all have the specificity of being potentially extractible from biomass in their catechol forms, by involving electrochemistry calling either to Li, Na or Mg.

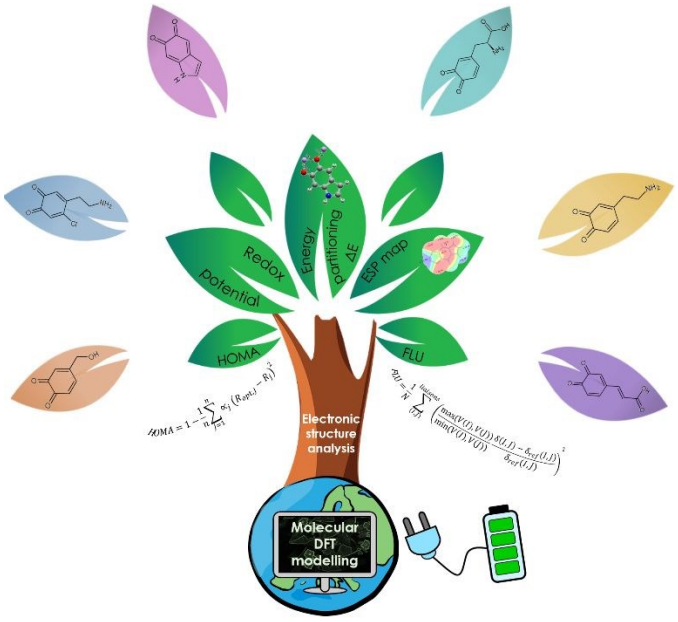

Figure 1. Illustration of the strategy, specific tools and type of materials considered in this work, encompassing: i) molecular electrostatic surface potential (ESP) maps to identify the preferred potential location of metal-ions ii) electron delocalization indices (*i.e.* the Harmonic Oscillator Model of Aromaticity (HOMA) and Aromatic Fluctuation index (FLU) descriptors) to account for the variation of the quinoidic ring stability as a function of reduction stage, along with iii) the partitioning of the global energy of the molecule into atomic or atomic group energy contributions, which leaves the possibility to shed light on the predominant role played by some moieties on the global stabilization/destabilization features or to account for the balance between some competitive effects and finally iv) net atomic charges able to give indication either on charge transfers or on electrostatic interactions.

This work is organized as follows: in Section 2 and Section 3 details about the chemical structures of the considered quinone families and the theoretical methods are given, respectively. The results and discussion are presented in Section 4 and the concluding remarks in Section 5.

With the objective of reaching a level of understanding corresponding to quantitative structure–activity relationships, we

not only predicted redox potential of the selected set of redox-active molecules but also attempted to unveil the understanding of their relative aptitudes with respect to these electrochemical features through differences of quantities before and after the reduction process (ΔP, where P represents the property). In view of reaching this objective, the various sub-sections of the results and discussion part are used in order to present, in a progressive manner, the potential interest or usefulness of the various tools employed in this investigation: i) ESP maps were solely used to predict the preferential positioning of the metal cation after reduction in the vicinity of the carbonyl centres belonging to the *o*-quinone ring; ii) delocalization indices ΔHOMA, ΔFLU were employed to evaluate exclusively the ring aromatization, which is quite consequent but not sufficient to rationalize the redox potentials ranking; iii) then, ΔE values were estimated in order to account for the relative extents of energy variations as a function of atomic/molecular groups. These latter correspond to an important tool of the arsenal to consider here by proving that the major variations concern the ring (since other contributions are of lower extent in absolute values) whereas global ΔE only can account of the higher redox voltage for two compounds whatever the metal cation type. Additionally, it was demonstrated that the decomposition in various ΔE components for a same system enable the appreciation of the effects induced by slightly modifying the functionalization. At a final stage (iv), we furthermore considered the net atomic charges to account for the electrostatic interactions in our metal-anion clusters, and discovered that they could play a significant part in the relative extent of the observed redox potentials as well, especially by introducing a switching between Li/Mg systems from the viewpoint of their relative stabilization (and thus their redox potentials). The detailed definition of each of the above-mentioned parameters (ESP, HOMA, FLU, E) is given in Section 3.

2. Investigated systems

View Article Online
DOI: 10.1039/D0CP02045A

A possible way to access quinones directly extracted from biomass relies on the transformation of catechols (corresponding to a fully reduced form of 1,2-benzoquionone), which are widely distributed in nature, in both plant and animal systems into their oxidized *o*-quinone forms. Within two-electron two-proton oxidation processes quinones can indeed be formed via intermediates (semiquinones). Within this family, we selected in our investigations the following systems: (4-(hydroxymethyl)catechol) (HMC);[33], dopamine (DA)[34], 5,6-dihydroxyindole (DHI) or dopamine lutine[35], 2-chloro-4,5-dihydroxyphenylalanine or Cl-dopamine[36], 3,4-dihydroxy-L-phenylalanine or *L*-dopamine (levodopa or *L*-DA)[37,38] and caffeic acid (CA), which belongs to very commonly occurring phytochemicals, and can be found for instance in the bark of *Eucalytus globulus*[39] and the herb *Dipsacus asperoides*[40], in the freshwater fern *Salvinia molesta*[41] and in the mushroom *Phellinus linteus*[42] (Figure 2). Within this series, it can be highlighted that the seeds of a tropical legume, Mucunia pruriens, contain large amounts of L-DA[43]. This compound is famous especially as main drug in the Parkinson's disease, antidepressant and as psychoactive. It also serves as a fodder plant, such as ersatz coffee (caffeine), and as antagonist of snake venoms. *L*-DA is furthermore the source of natural macromolecules including melanins. Besides, *L*-DA, which can be oxidized to *o*-quinones, easily undergoing an oxidative coupling, lead to the crosslinking of peptide chains. Insoluble in most common solvents, these latter provide to Mytilus edulis (blue mussel) the well-known exceptional adhesion force (*i.e.* adhesion strength up to 800,000 N/m^2 on polar surfaces and 30,000 N/m^2 on non-polar surfaces). For the sake of simplicity, the investigated quinones will be simply denominated in the following study as: HMQ, DOPA, IQ, Cl-

View Article Online
DOI: 10.1039/D0CP02045A

DOPA, *L*-DOPA, and CQ, corresponding, respectively, to 4-(hydroxymethyl)-1,2-benzoquinone, Dopamine-*o*-quinone, Indole-5,6-quinone (which can be obtained from the cyclisation of Dopamine-*o*-quinone), 3-Chloro-Dopamine-*o*-quinone, *L*-dopaquinone and Caffeoquinone (Figure 2).

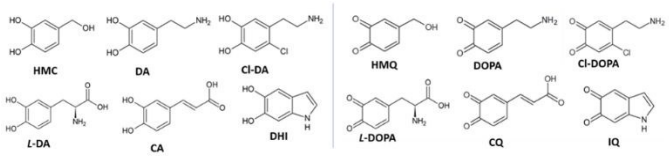

Figure 2. Catechols systems (Left) and corresponding *ortho*-quinones investigated (Right).

3. Computational Methods

In this study, we report the fundamental redox characteristics of the above-mentioned *o*-quinone derivatives as well as an accurate examination of the major stabilization/destabilization effects accounting for the observed ranking. In addition to the Li^+ based systems and with the objective of focusing on merged advantages of next-generation "beyond-lithium" battery chemistry including both organic compounds and other fashionable monovalent or abundant multivalent ions, a comparison with the Na^+ and Mg^{2+} based *o*-quinones was performed. Such accurate examination on the differentiation induced by tuning the nature of intercalating element indeed appears to be crucial in link with the possibility of utilizing multivalent ions for redox-active quinone systems based on catechols, which has been demonstrated recently[44], with studies related to electrochemical storage systems calling to naturally derived melanin pigments (including indole moieties in their structure).

The first purpose of our quantum chemistry investigations was to evaluate the thermodynamic properties of the set of various organic molecules and complexes. Gaussian09.D01 package[45] was adopted to perform these computations. Structures were fully optimized at the M062X level of theory with the polarized triple ζ basis set 6-311+G(2d,2p) by using a very tight criterion of convergence and confirmed as true local minima by vibrational frequency analyses (carried out at the same computational level to evaluate the Gibbs free energy at 298K). Solvent effects were taken into account by means of a polarizable continuum model, *i.e.* Solvation Model based on Density (SMD)[46], with acetonitrile as solvent (ε = 37.5). Except for IQ species which is characterized by a single conformation, Potential Energy Surfaces (PES) were evaluated for all other molecules and complexes to identify the possible various conformers with respect to the chemical group attached to the *o*-quinone ring. As already described in previous works[12,13,14,47], the redox potential was calculated through the Nernst equation:

$$E = \frac{-(\Delta G)}{nF} \quad (1)$$

where E is the voltage, ΔG is the reaction free energy, n is the number of electrons transferred in the reaction, and F is Faraday's constant determined before getting the final considered redox potential relative to the Li^+/Li reference electrode.

We adopted two hypotheses of compounds undergoing either a one-electron (one monovalent counter-ion) or a two-electron (two monovalent counter-ion or one divalent counter-ion) reaction, due to the fact that both cases have been observed in experiments according to the studied compound (with failure to reach the doubly reduced state in some cases). The calculations were thus performed for "initial" states ("monomers" corresponding to the quinones mentioned in Figure 2) as well as for "intermediate"

DOI: 10.1039/D0CP02045A

states (involving a complex between the singly reduced molecule – *i.e.* a semiquinone – and one Li^+ or one Na^+) and for "final" states (linked to the double reduction of the two carbonyl entities from the quinone compound, which are interacting with either two alkaline cations or with one Mg^{2+}).

Following the DFT computations, various indicators of electron delocalization based on geometrical or electronic structure features were estimated. Procedures probed as efficient to rationalize ranking and differentiation of electrochemical features were also adopted[12,13,14]. The characterization of aromaticity and of electron delocalization through the HOMA and FLU descriptors uses, respectively, pure geometry features and quantities obtained through a Quantum Theory of Atoms in Molecules (QTAIM) space partitioning and integration within each atomic basin[48]. HOMAs[49] provides a measure of the bond distances deviation in the ring relative to an aromatic model. The HOMA value for a n-member unsaturated ring is evaluated through the formula:

$$HOMA = 1 - \frac{1}{n}\sum_{j=1}^{n} \propto_j (R_{opt,j} - R_j)^2 \qquad (2)$$

where R_j denotes the various bond lengths taken into account for the calculation, *n* is the number of bonds in the ring; α_j is a normalization constant fixed to give HOMA = 0 for a model non-aromatic system and HOMA = 1 for a system with all bonds equal to the optimal value, $R_{opt,j}$, which is assumed to be reached in fully aromatic systems. HOMA is therefore equal to 1 for benzene and 0 for a model non-aromatic system, like the Kekulé form of benzene. HOMA may eventually become negative for heavily substituted rings or in the case of anti-aromatic systems. This model was then adapted to include several different types of bond types, *i.e.*, CN, CO, CP, CS, NN, and NO and, for the specific case of hetero-π-electron systems, a further modification of the HOMA index was proposed[50,51]. In the present study, the following α values were taken into account for CC bonds and CN bonds, respectively: α_{CC} = 257.70 and α_{CN} = 93.52. We used for CC bonds $R_{opt,CC}$ = 1.388 Å, where CC is the bond distance in benzene and for CN bonds: $R_{opt,CC}$ = 1.334 Å. In this work, we estimated HOMA for initial, intermediate and final state and quantities Δ(intermediate state – initial state) and Δ(final state – initial state), were then presented. Indeed, as stated above, the redox potential is linked to the difference of G values between oxidized and reduced forms. Therefore, the HOMA values for either reduced or oxidized states are clearly insufficient to account for any extent of redox voltage whereas ΔHOMA between the two forms, directly indicating the electron delocalization change provided by reduction process, is the key quantity to consider for the rationalization, at least partly of the values found for this quantity (other contributions (functional groups (FGs)/redox centres being naturally also involved), but estimated thanks to a further tool: the global molecular energy partitioning, presented hereafter).

The other aromaticity criterion, FLU, depends not only on the amount of electron sharing between contiguous atoms, which should be substantial in aromatic molecules, but also on the similarity/dissymmetry of electron sharing between adjacent atoms [52]. This parameter is expressed as the deviation from a reference value of the electron pair sharing over a bond in a ring according to:

$$FLU = \frac{1}{N}\sum_{(I,J)}^{bonds}\left(\frac{\max(V(I),V(J))\delta(I,J) - \delta_{ref}(I,J)}{\min(V(I),V(J))\quad \delta_{ref}(I,J)}\right)^2 \qquad (3)$$

where V is the atomic valence in the QTAIM framework and for which the sum is performed over the whole set of atoms *I* and *J* for all considered N bonds, *i.e.:*

$$V(I) = \sum_{I \neq J}^{all\ atoms}\delta(I,J) \qquad (4)$$

View Article Online
DOI: 10.1039/D0CP02045A

Contrary to HOMA, FLU approaches zero for highly aromatic systems and largely deviates from zero for non-aromatic ones. δ_{ref} = 1.386, was taken as reference value for evaluating FLU indices. Like for HOMA values, we focused on the variations of this quantity among the three considered states to account for the stability evolution produced through the reduction process.

Besides characterizing the electron delocalization in the rings, it is possible to evaluate the atomic/functional group QTAIM energies (or Bader's energy, E)[48,53] and their evolution upon the electrochemical reaction (ΔE). Such energy partition allows to identify those atom(s)/group(s) of atoms or rings that play a significant role in the energy stabilization/destabilization during the reduction process. One may so estimate how much a given atomic or molecular moiety concur or oppose the ring aromatic/antiaromatic energy modulation within the process probed with ΔHOMA and ΔFLU. Like for HOMA and FLU quantities, we considered ΔE evolutions, which are able to account for the variations occurring not only on the rings (already examined through these above-mentioned delocalization descriptors) but also on all other portions of the molecule. Indeed, variations of each atomic group can be either stabilizing or destabilizing and can counter-balance the stabilization occurring for the ring when the quinone moiety is transformed into its corresponding reduced form. Thanks to this approach a complete overview of the various roles played by specific parts of the molecule is reachable.

Additionally, atomic electron charges/electron spin populations were collected through slightly modified versions of the Extreme and PROMEGA programs[54] applied to the solvated systems wavefunction.

Finally, we considered maps of molecular electrostatic potential. These electron isodensity surfaces mapped with the electrostatic potential energy felt by an electron moved over this surface (*i.e.* Electrostatic Surface Potential, (ESP)) maps display the potential that a unit positive charge would experience at any point of the surface due to the electron and nuclear distribution in the molecule. In such maps, red areas indicate the lowest electrostatic potential energy and blue is linked to the highest one. Intermediate colours represent intermediary electrostatic potentials. Therefore, area of low potential, red, are characterized by a relative abundance of electrons while areas of high potential, blue, are experiencing a relative depletion of electrons. Accordingly, the *minima* of the ESP maps will likely coincide with the sites of preferred *electrophilic* attack to the system under investigation. Therefore, ESP maps may give precious indication on the preferential location of metal cation during the electrochemical process.

4. Results and discussion

4.1 Structures and Electrostatic Surface Potential (ESP) maps

The search for conformational preference was systematically undertaken through PES theoretical calculations for each quinone system (either in monomer form (initial state) or through complexes involving one (intermediate state) or two (final state) monovalent metal cations or one divalent cation for the final state of Mg-based systems). A complete description and a comparison of structural and energetical features among most prominent conformers is reported in the ESI. Most stable conformers, which were used for the calculation of redox potentials are displayed in Figure 3 and Fig SI1 and SI2, for Li, Na-, Mg- based systems, respectively. ESP maps (presented on Figure 4 and Fig SI3 and SI4 for Li, Na-, Mg- based

Journal Name ARTICLE

View Article Online
DOI: 10.1039/D0CP02045A

systems, respectively) were exploited to predict and rationalize prevalent cation positioning and, in the case of the intermediate state, also to assess the role of the nature of the monovalent cation.

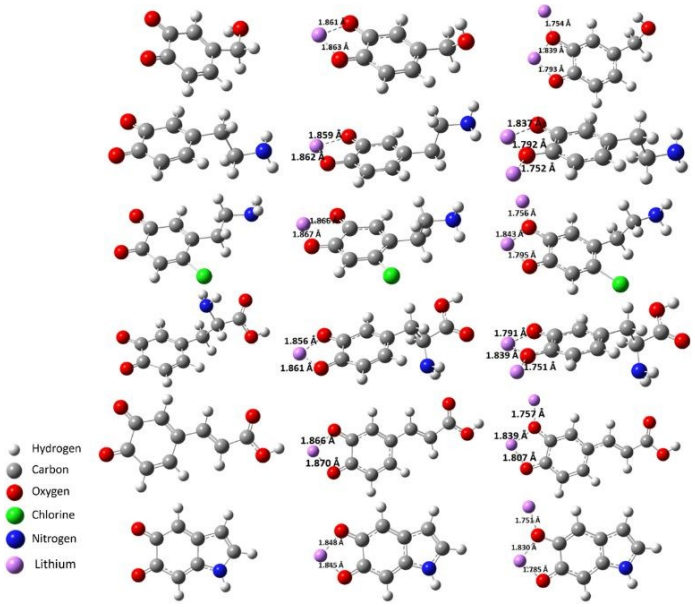

Figure 3. Most stable structures for Li-based systems. Left: monomer (initial state); Middle: complex involving one Li^+ cation (Single reduction); Right: complex involving two Li^+ cations (Double reduction); From Top to Bottom: HMQ, DOPA, Cl-DOPA, *L*-DOPA, CQ and IQ.

In this section, we first discuss in detail the ESP analysis for the case of the IQ system and of its singly and double charged complexes involving either alkaline or magnesium cations, as a representative example. Main features for ESP analysis are also gathered here in the case of other systems by focusing on the common points or distinctions that could occur with respect to main trends observed for IQ. The details of such analysis are also carefully described in the ESI system by system for a more thorough interpretation.

The ESP map for the initial form of IQ exhibits, within the sole red area appearing in the neighbourhood of the redox centres, a minimum at: -68.70, in the vicinity of the carbonyl groups, located at half-way from both Oxygen atoms. Not surprisingly, in the intermediate form, the alkaline or Mg atom thus preferentially interacts with *o*-quinone ring (6MR) by forming a bidentate bonding type involving the two O-atoms from the initial carbonyl groups.

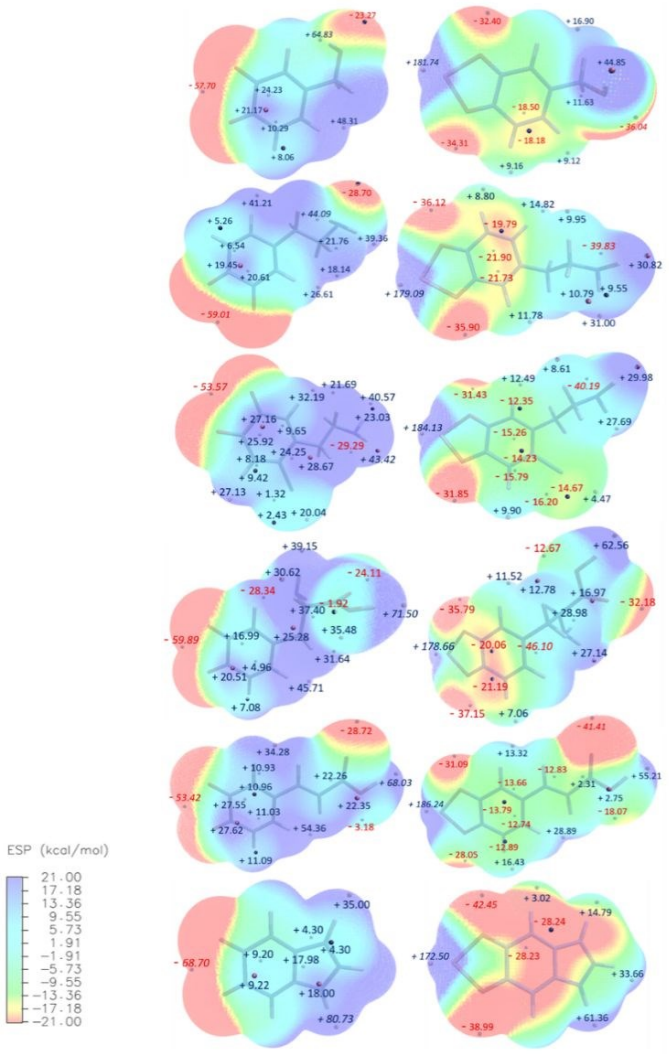

Figure 4. Most stable structures for Li-based systems. Left: monomer (initial state); Middle: complex involving one Li^+ cation (Single reduction); Right: complex involving two Li^+ cations (Double reduction); From Top to Bottom: HMQ, DOPA, Cl-DOPA, *L*-DOPA, CQ and IQ. The colour scale applies to all compounds/states.

With Li- and Na-based species, the calculated interatomic distances amounts to 1.85 Å (for Li^+) and 2.20 Å (for Na^+). The final form of the Mg-based system, which naturally involves only one Mg in between the two O linked to the 6MR of carbons, is characterized

View Article Online
DOI: 10.1039/D0CP02045A

by a Mg-O interatomic distance of 1.91/1.92 Å. The ESP map of the intermediate form presents only two minima (at: -42.45 and -38.99 in the case of Li^+ and at: -46.04 and -42.34 for Na^+-based systems, respectively), which are almost symmetrically located at right and left from the bidentate O-Li-O group. The final form of the IQ (with Li or Na) is obtained by introducing a further alkaline atom which, according to the ESP map of the intermediate state, is expected to place itself on the ESP minimum region opposite to the N of the pyrrole ring fused to the 6MR. Indeed, the most stable final form, I, (among the two possible conformers, I and II, see ESI) agrees with this hypothesis in both cases (Li^+- and Na^+- based systems). Both I and II are characterized by alkaline cation-oxygen interatomic distances of about 1.75 Å and 2.12 Å for Li- and Na-based systems, respectively, while we can notice a slight asymmetry introduced in the preserved bidentate moiety with interatomic distances evaluated at (1.79 Å, 1.83 Å) and (2.15 Å, 2.19 Å) with Li- and Na-species, respectively. When the additional alkaline atom interacts with the Oxygen from the carbonyl group situated on the other side (final form II, see ESI, Figure SI-5) the structure is less stable by about 0.9 and 0.8 $kcal.mol^{-1}$ for Li- and Na-based compounds.

For the other systems in their most stable form, the general trend of finding an ESP minimum in the vicinity of the carbonyl groups of the initial state, roughly located at half-way from both Oxygen atoms, is always preserved. Focusing on the monodentate systems, for L-DOPA and CQ, which both have the specificity to bear an FG containing a carbonyl, the ESP minima do not concern solely the *o*-quinone part of the molecule, since a red area is observed also in the vicinity of this potential further redox centre. With respect to the differentiation in ESP minima extent between the two values in the neighbourhood of Li^+, we observe a Δ(ESP) of ~ 3.0 and 1.4 for CQ and L-DOPA respectively. In both cases, the positioning of the further Li^+ coincide with the deepest ESP minimum. For one-Na^+ complex, such trend is still preserved with a preference of Na^+ for the side where the deepest minimum is located (with Δ(ESP) of ~ 3.2 and 1.6 for CQ and L-DOPA). For L-DOPA and CQ systems, another interesting feature concerns the extent of the ESP minimum in the vicinity of the carbonyl belonging to the FG with a clear rising trend by switching from Li- to Na-series. The following values, -41.41/-44.58 and -32.18/-34.50 in the case of CQ and L-DOPA compounds, for the Li^+/Na^+ systems, are indeed observed, respectively. Concerning the HMQ, DOPA and Cl-DOPA molecules in their monodentate form (all devoid of carbonyl in the FG), we can observe systematically a similar phenomenon of absolute values raising of ESP minima by switching from Li to Na systems. For all these compounds, the Δ(ESP) between both sides of potential positioning of the cation in the neighbourhood of carbonyl groups of the *o*-quinone are lower than the differences observed in the case of CQ and L-DOPA. For the DOPA system for instance, the Δ(ESP) are lying in between ~ 0.2 and 0.4 and the privileged positioning of the cation occurs at the deepest ESP minimum. The almost constant and small Δ(ESP) value of 0.4 for Li^+ and Na^+ leads instead to a cation positioning which is inconsistent with the lowest ESP value in the case of Cl-DOPA. The HMQ system also behaves similarly despite a larger extent of differentiation between both sides ($1.9<\Delta(ESP)<2.2$).

View Article Online
DOI: 10.1039/D0CP02045A

4.2 Redox potentials

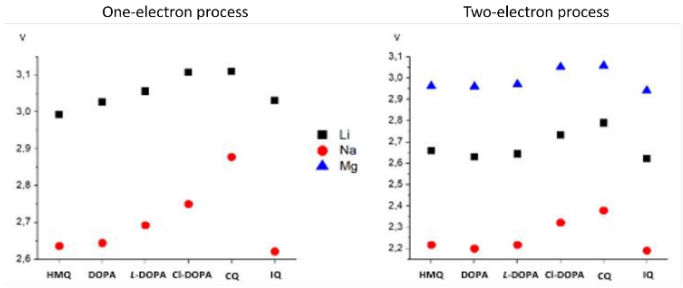

Figure 5. Calculated redox potentials, V in Volts (*vs.* Li^+/Li). Left: single reduction; Right: double reduction.

Redox potentials characterizing the reduction process for the set of investigated systems (lying as a whole within the range 2.2–3.1 V *vs.* Li^+/Li) are displayed in Figure 5. Highest voltages are found for CQ and Cl-DOPA whatever the intercalation type (1 electron/2 electrons) and the nature of metal-ion ($Li^+/Na^+/Mg^{2+}$) involved, yet with slight differentiation with respect to all other molecules. Globally, the metal-ion effect induces more differentiation in the electrochemical features than the modulation in FGs in the investigated set of quinones deriving directly from naturally occurring compounds. The observed trends demonstrate that the various *o*-quinone behave quite similarly as a function of the metal-ion. Systematically, for both the one- and two-electron processes, the redox potentials are characterized by the following ranking: Sodium (Na)- based values are inferior to Lithium (Li)- counterpart values while Magnesium (Mg)- magnitudes are always much higher than Lithium ones and, a fortiori, than Sodium ones. This observation is consistent with the work of Chung *et al.*[55], who demonstrated the following ranking $La^{3+} > Mg^{2+} > Ca^{2+} > Li^+ > Na^+ > K^+$ for the positive shift of reduction potential of a few analogues of calix-[4]-arene diquinone. Our results agree as well with the work of Patil *et al.*[56] who studied polymers bearing catecholato–metal cation complexes and who observed quite substantial shifting towards higher redox voltages for complexes involving stronger interactions (*i.e.* $M^+ < M^{2+} < M^{3+}$). For the one-electron process, the differences between Na- and Li-based systems lies between 0.23 (for CQ) and 0.41 V (for IQ). For HMQ, Cl-DOPA and L-DOPA, the extent of 0.36 V is found between both M^+-series whereas it is slightly higher (0.38 V) for DOPA. With respect to the two-electron process, the magnitude of the difference between Li and Na-based systems is slightly higher (0.41-0.44 V), with highest difference for HMQ (0.44 V) and then IQ, DOPA and L-DOPA (0.43 V). For a given type of metal-ion and system, the one-electron reduction is giving rise to slightly higher values of redox potentials (2.6–3.1 V *vs.* Li^+/Li for Li/Na- based systems) than the two-electron process (2.2–2.8 V *vs.* Li^+/Li for Li/Na-based systems and up to 3.1 for Mg compounds). For the one-electron Li-process, the lowest and highest potentials appear for HMQ/DOPA/IQ and CQ compounds, respectively, although the differentiation appears to be very small (ΔV = 0.1 V). Comparatively, the ΔV between the extrema in the Na-series of single reduction is higher, being equal to ΔV = 0.3 V, with the lowest and highest potentials still observed for HMQ/DOPA/IQ (2.6 V *vs.* Li^+/Li) and CQ (2.9 V *vs.* Li^+/Li) compounds, respectively. Concerning the two-electrons process, a difference of ΔV = 0.3 V is noticed within the whole series of Li^+-systems, the lowest/highest voltage being: 2.6 (for IQ/DOPA/L-DOPA) and 2.9 V (for CQ) *vs.* Li^+/Li, respectively. Slightly higher redox potentials are observed for the double reduction involving magnesium (lying in between 2.9 (for IQ) and 3.1 (for Cl-DOPA and CQ) *vs.* Li^+/Li).

4.3 HOMA/FLU evolutions upon the reduction process

As a first indicator of modulation of chemical bonding features upon reductions, HOMA and ΔHOMA were considered. Beyond HOMA analyses, change in ring delocalization features during the redox process were also probed through FLU evaluations. HOMA and FLU data along with their corresponding changes upon reduction,

ΔHOMA and ΔFLU (corresponding to the change Δ(intermediate state – initial state) and Δ(final state – initial state), for the single and double reduction, respectively), are listed in Table 1 and represented on Figure 6. A positive/negative value of ΔHOMA/ΔFLU indicates a stabilization during the electrochemical process.

Table 1. Local aromaticity HOMA and FLU indexes for XMR rings (X=6, R1; X=5, R2 (IQ system only)) and their changes ΔHOMA and ΔFLU upon one-or two electron reduction process. The changes correspond to Δ(intermediate – initial) and Δ(final – initial) states, for the single and double reduction, respectively.

System Cation/State	HOMA, R1 (R2)	ΔHOMA, R1 (R2)	FLU, R1 (R2)	ΔFLU, R1 (R2)
HMQ				
None/initial	-1.23	–	0.080	–
Li/intermediate	0.41	1.64	0.029	-0.051
Li/final	0.85	2.08	0.008	-0.072
Na/intermediate	0.33	1.56	0.030	-0.050
Na/final	0.76	1.99	0.009	-0.071
Mg/final	0.89	2.12	0.006	-0.074
DOPA				
None/initial	-1.22	–	0.080	–
Li/intermediate	0.42	1.64	0.028	-0.052
Li/final	0.86	2.08	0.008	-0.072
Na/intermediate	0.34	1.56	0.029	-0.051
Na/final	0.76	1.98	0.009	-0.071
Mg/final	0.88	2.10	0.007	-0.073
Cl-DOPA				
None/initial	-1.18	–	0.079	–
Li/intermediate	0.44	1.62	0.028	-0.051
Li/final	0.86	2.04	0.011	-0.068
Na/intermediate	0.36	1.54	0.029	-0.050
Na/final	0.76	1.94	0.011	-0.068
Mg/final	0.89	2.07	0.008	-0.071
***L*-DOPA**				
None/initial	-1.22	–	0.081	–
Li/intermediate	0.43	1.65	0.028	-0.053
Li/final	0.85	2.07	0.008	-0.073
Na/intermediate	0.34	1.56	0.029	-0.052
Na/final	0.76	1.98	0.010	-0.071
Mg/final	0.88	2.10	0.007	-0.074
CQ				
None/initial	-1.17	–	0.080	–
Li/intermediate	0.38	1.55	0.030	-0.050
Li/final	0.80	1.97	0.012	-0.068
Na/intermediate	0.30	1.47	0.032	-0.048
Na/final	0.69	1.86	0.015	-0.065
Mg/final	0.87	2.04	0.009	-0.071
IQ				
None/initial	-1.37 (0.13)	–	0.071 (0.036)	–
Li/intermediate	0.23 (0.58)	1.50 (0.45)	0.029 (0.022)	-0.042 (-0.014)
Li/final	0.71 (0.77)	2.08 (0.64)	0.014 (0.013)	-0.057 (-0.023)
Na/intermediate	0.15 (0.59)	1.52 (0.46)	0.030 (0.022)	-0.041 (-0.014)
Na/final	0.58 (0.77)	1.95 (0.64)	0.016 (0.012)	-0.055 (-0.024)
Mg/final	0.74 (0.77)	2.11 (0.64)	0.013 (0.013)	-0.058 (-0.023)

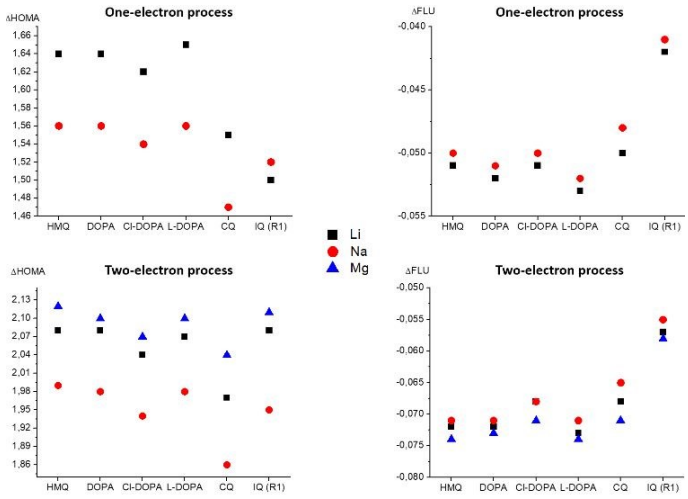

Figure 6. Variations of HOMA (Left) and FLU (Right) values (*i.e.* ΔHOMA or ΔFLU) upon reduction process Top: one-electron process; Bottom: two-electrons process.

HOMA values for 6MR, in the initial forms (monomers) are all largely negative (-1.17 – -1.37) and similar, in link with the quinoidal initial form while these HOMA become all positive after the

View Article Online

DOI: 10.1039/D0CP02045A

electrochemical process. Large and positive ΔHOMA values for this ring indeed show that such initial bond length inequality is partially released upon reduction. As a whole, ΔHOMA lies in between 1.47 and 1.65 for intermediate forms (after the one-electron process) and in the range: (1.86 – 2.12) for the final forms (after the two-electron reduction). The quite similar values for all compounds in a given type of form (either initial, intermediate or final) seem to indicate that they may exploit similar electron delocalization patterns, the systematic lower extent of HOMA for the intermediate state compared to the final state being linked to its lower aromatic character. Focusing on the incidence of the nature of the metal-ion effect, we can observe that whatever the compound, the stabilization is always slightly higher for the Li-based compounds compared to the Na-based counterparts. A larger stabilization is systematically observed for Mg-based compounds compared to Li-based ones. This trend is consistent with the rising redox potential for the Na < Li < Mg series and may thus eventually contribute – at least partly – to this observed shifting towards higher redox potentials. In the case of IQ, the 5MR exhibits quite similar trends with respect to HOMA values observed for 6MR 1, with ΔHOMA equal to 1.50–1.52 and to 1.95–2.11 for the intermediate and final forms, respectively. In agreement with HOMA trends, FLU values for the 6MR of the initial state are very similar, in the range: 0.071–0.081 for all compounds. Magnitudes of FLU clearly decrease upon reduction for this ring moiety, with ΔFLU equal to - 0.042 – - 0.051 and - 0.055 – - 0.074 for a one- and two-electron process, respectively. This observation is consistent with ΔHOMA values and tend to prove that 6MRs have enhanced their aromatic character and thus their energy stabilization compared to the initial state (and even more so after a double reduction than after a single one). This latter aspect clearly constitutes the most relevant phenomenon. Comparatively to the 6MR, magnitudes for ΔFLU in the case of the 5MR of IQ are much less important. On the other hand, the change in the nature of metal-ion in the vicinity of the redox centres still induces a differentiation that was already observed for the ΔHOMA (although less pronounced), higher stability being observed within this ranking: Mg- > Li- > Na-based compounds.

Apart from these ring delocalization features, other potential contributions originating from the substituent, the oxygen from the redox centres, etc have to be considered since these trends could eventually have synergistic effects or counter-balance these aspects observed solely based on the 6MR stabilization features. An overview of the various possible stabilization or destabilization contributions is provided in the next section.

4.4 Molecular energy partitioning into additive atomic group contributions

After the previous examination of the ring's relative electron delocalization features and evolution, we conducted a complementary Bader's energy (E) decomposition analysis aimed at evaluating the relative extent of the various energy changes occurring for the various atomic groups of each *o*-quinone upon the reduction process. The considered difference in energy, ΔE, corresponds to Δ(intermediate state – initial state) and Δ(final state – initial state), concerning the single and double reduction, respectively, for each of the considered moieties. By focusing on the stabilization/destabilization (*i.e.* negative/positive ΔE, respectively) of the whole pieces of the molecular entities afforded by the electrochemical process, this procedure enables a thorough insight on the relative role played by the various sections of the molecular

entities and clearly goes beyond the sole consideration of the 6MR delocalization presented in the previous section. The ΔE (in Hartree (Ha)) evolution after either one- or two-electron(s) process of i) the 6MR, ii) the FG, iii) the "O1" species (*i.e.* O atoms from the redox centres, binded to the 6MR), iv) the "O2" species (*i.e.* O atoms belonging to the FG when they are present), as well as v) N and Cl atoms (whenever they are occurring in the FG(s) or 5MR of IQ) is gathered in Table 2 and displayed in Figure 7 (for the case of IQ, the 5MR was considered in these graphs as the FG).

Table 2. Variation in Bader's energy (ΔE values, in Hartree (Ha)) upon one-electron (SR, single reduction) or two-electron (DR, double reduction) processes for Li-, Na- and Mg- based compounds. These ΔE values concern the 6MR (R1), the 5MR (R2; only for IQ system), the functional group (Funct. Group), the O atoms from the redox centres (O1) binded to the 6MR, the O atoms (O2) of the functional group (if present), the N and Cl atoms (if present in the functional group(s) or in the 5MR of IQ). All energies are in Hartree (Ha).

System Cation /Reduc-tion	ΔE, R1 (R2)	ΔE (Funct. Group)	ΔE (O1)	ΔE (O2)	ΔE (N)	ΔE (Cl)
HMQ						
Li/SR	-0.311	-0.034	0.104	0.016	–	–
Li/DR	-0.547	-0.078	0.178	0.009	–	–
Na/SR	-0.206	0.003	0.182	0.044	–	–
Na/DR	-0.336	-0.007	0.327	0.058	–	–
Mg/DR	-0.496	-0.031	0.262	0.018	–	–
DOPA						
Li/SR	-0.314	-0.034	0.107	–	-0.010	–
Li/DR	-0.548	-0.083	0.188	–	-0.023	–
Na/SR	-0.200	0.013	0.191	–	0.011	–
Na/DR	-0.325	0.008	0.345	–	0.017	–
Mg/DR	-0.487	-0.026	0.273	–	-0.000	–
Cl-DOPA						
Li/SR	-0.309	-0.025	0.109	–	-0.006	-0.044
Li/DR	-0.534	-0.056	0.200	–	-0.013	-0.109
Na/SR	-0.258	-0.012	0.151	–	0.001	0.009
Na/DR	-0.422	-0.028	0.285	–	-0.000	-0.001
Mg/DR	-0.542	-0.041	0.236	–	-0.007	-0.057
***L*-DOPA**						
Li/SR	-0.303	-0.049	0.110	-0.012	-0.005	–
Li/DR	-0.524	-0.123	0.197	-0.037	-0.012	–
Na/SR	-0.218	0.031	0.175	0.028	0.010	–
Na/DR	-0.351	0.033	0.323	0.039	0.015	–
Mg/DR	-0.496	-0.030	0.258	0.005	0.003	–
CQ						
Li/SR	-0.298	-0.050	0.096	-0.007	–	–
Li/DR	-0.517	-0.124	0.163	-0.016	–	–
Na/SR	-0.212	0.017	0.159	0.035	–	–
Na/DR	-0.343	0.008	0.282	0.068	–	–
Mg/DR	-0.494	-0.046	0.232	0.019	–	–
IQ						
Li/SR	-0.312 (-0.034)	–	0.094	–	-0.011	–
Li/DR	-0.568 (-0.088)	–	0.172	–	-0.016	–
Na/SR	-0.206 (0.032)	–	0.173	–	0.012	–
Na/DR	-0.354 (0.046)	–	0.322	–	0.025	–
Mg/DR	-0.514 (-0.008)	–	0.255	–	0.003	–

Regardless of the system and whatever the reduction type or nature of metal-ion involved, the energy stabilization upon reduction is dominated by the stabilization of the 6MR, which is only partially opposed by the concomitant destabilization of the quinonic O1 atoms. All other energy contributions from FG, N and Cl are often stabilizing but definitely smaller in magnitude. Yet, they may turn to be decisive in determining the observed ranking of the diverse molecules in terms of redox potential. A more detailed analysis for the various systems as a function of the metal-ion and reduction process is therefore required and follows below.

View Article Online
DOI: 10.1039/D0CP02045A

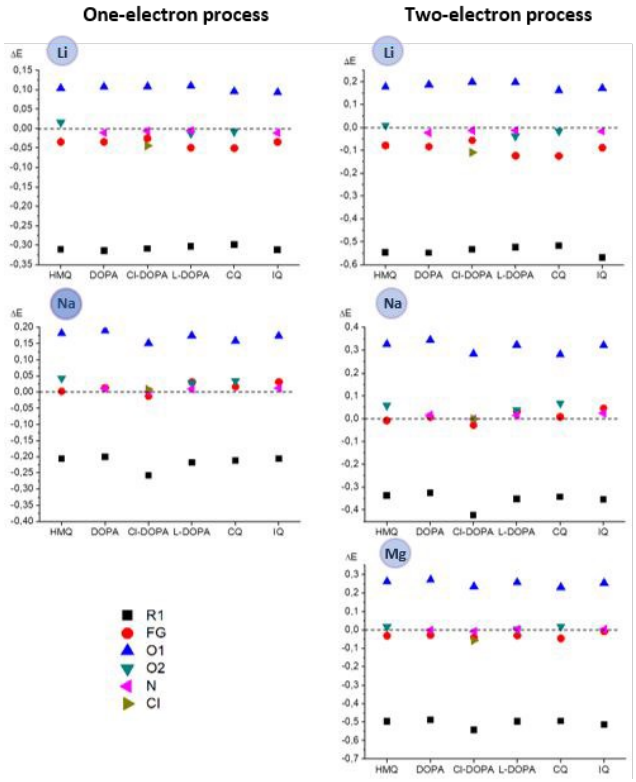

Figure 7. Representation of Bader's variation in energy, ΔE (in Hartree (Ha)), upon one-electron (Left) or two-electrons (Right) process for Li- (Top), Na- (Middle) and Mg- (Bottom) based compounds concerning the 6MR ("R1"), the functional group (FG), the "O1" species corresponding to the O atoms from the redox centres, binded to the 6MR, the "O2" species (*i.e.* O atoms belonging to the FG when they are present), N and Cl atoms (whenever they were occurring in the FG(s) or 5MR of IQ). For IQ, the second ring (5MR) has been introduced in this graph "FG" for the sake of conciseness.

Regarding the single reduction involving Li^+ species, the 6MR energy stabilization (negative ΔE values) is about three times larger in magnitude than the O1 destabilization energy (positive ΔE values). The O2 species are systematically stabilizing in all compounds except with HMQ, which introduces a slight destabilization originating from this kind of atoms. The ΔE values of all compounds for the whole set of other inspected pieces of the molecules are always negative, thus indicating their contribution to the stabilization effect, although at a much lower magnitude compared to the ΔE due to 6MR. In particular, we can observe that the Cl and N are always experiencing a stabilization whatever the case, the Cl atom being however much more stabilized than the N atom in the case of Cl-DOPA. The FG is always stabilized during the reduction process, but with much lower extent than the one produced by the 6MRs. A small but noticeable differentiation for the FG is produced as a function of the compound nature, the larger stabilization being obtained in this ranking: CQ > L-DOPA > HMQ ~ DOPA ~ IQ > Cl-DOPA. One of the main learning that can be gained from the accurate examination of the overall ΔE trends during the Li one-electron process is that the 6MR evolution by itself is not sufficient to account for the ranking of the diverse molecules in terms of redox potential. Indeed, the highest voltage compounds (CQ and Cl-DOPA) are in fact characterized by values of ΔE for the 6MR that are lower in absolute value compared to the corresponding value for the lowest voltage HMQ molecule (in agreement with the above mentioned HOMA and FLU trends).

Globally, the observed ΔE evolution trends in the case of the two-electrons process for the Li^+-based compounds are qualitatively similar to those observed in the case of a single reduction, yet roughly multiplied by a factor two. It involves much larger extent of energy stabilization for the 6MR, along with a destabilization occurring through O1 atoms and finally a minor stabilization effect that can be ascribed to the FG.

Comparatively, the Na-single reduction process exhibits in fact more differentiation with the corresponding process involving Li^+. First, the 6MR, also predominant in all cases, is now of less extent (*i.e.* -0.200 – -0.258 against -0.298 – -0.314) and values of O1 destabilization are as high as those observed for the case of the Li^+ double reduction process (*i.e.* +0.151 – +0.191). As a further new feature, we can observe that several ΔE evolutions from the

View Article Online
DOI: 10.1039/D0CP02045A

heteroatoms constituting the FG and the FG itself (as a whole) become slightly positive, the most positive values being observed for *L*-DOPA, CQ and IQ (*i.e.* in this last case, FG being the 5MR). On the other hand, the ranking of the 6MR is slightly different from the one observed for the Li- single reduction.

In the case of the Na-double reduction process, the ΔE values are, as for the case of Li, roughly doubled relative to the one-electron process. The spreading of both O1 atoms destabilization and 6MR stabilization is however larger than for the single reduction. The heteroatoms produce a destabilization, which induces again higher ΔE for *L*-Dopa, CQ and IQ. The ranking of the 6MR stabilization is almost identical to the one characterizing the Na-one electron process, with highest value for the Cl-DOPA.

Compared to the Na two-electron process, the double reduction involving Mg exhibits concomitantly much higher extent of 6MR stabilization (*i.e.* -0.487 – -0.542), less destabilization of O1 atoms (*i.e.* +0.232 – +0.273), as well as an FG being as a whole either slightly stabilized or characterized by an almost null ΔE. As already observed for the Na reduction, the CQ and Cl-DOPA are still experiencing higher stabilization owing to the FG contribution and less destabilization of the O1 atoms than the other compounds.

Beyond these general considerations, the higher molecular redox voltage observed for CQ and Cl-DOPA is fully consistent with higher stabilization compared to the others, as explicitly demonstrated by summing up the various ΔE components upon the reduction process for all compounds having a meta functionalization: *i.e.* ΔE (Functional group) + ΔE (6MR ("R1")) (+ ΔE (Cl) for the specific case of Cl-DOPA) (Figure 8). Otherwise, the extent of global ΔE is clearly higher in absolute values for the two-reduction process compared to the one-electron process. Higher stabilization with Li-based systems compared to Na-ones was furthermore observed whatever the type of electrochemistry. These two aspects are consistent with predicted electrochemical features. Therefore, these global ΔE values constitute a good arsenal for deciphering main trends. By the way, it implies that focusing solely on the delocalization indicators (such as ΔHOMA, ΔFLU or ΔE (6MR ("R1")) is not sufficient by itself to account for redox potentials trends, especially when dealing with substituent effects.

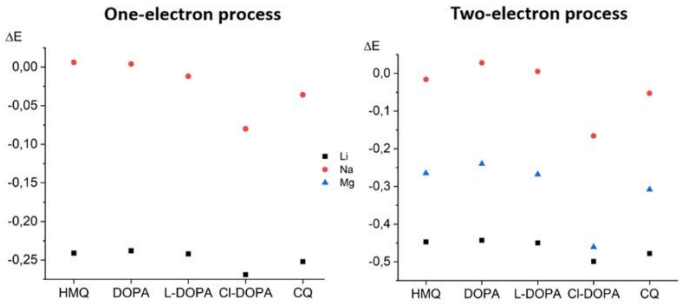

Figure 8. Representation of global Bader's variation in energy, ΔE (in Hartree (Ha)), upon one-electron (Left) or two-electrons (Right) process for Li-, Na- and Mg- based compounds obtained by summing up the 6MR ("R1"), the functional group (FG), the "O1" species corresponding to the O atoms from the redox centres contributions along with the Cl one in the case of Cl-DOPA.

Furthermore, the powerfulness of the energy partitioning approach (*i.e.* ΔE data gathered in Table 3) can be more specifically highlighted by the search for an evidence of redox potential differentiation between two compounds that are bearing the same FG at the same positioning except an additional Cl atom as further functionalization for one of them (*i.e.* DOPA and Cl-DOPA). Indeed, by focusing on the extent of stabilization provided by the 6MR (R1) upon the Li single reduction, it is slightly higher in the case of DOPA (-0.314) compared to the one of Cl-DOPA (-0.309), thus indicating that the sole consideration of this aspect would not be able to

Journal Name ARTICLE

View Article Online
DOI: 10.1039/D0CP02045A

rationalize the higher redox voltage of Cl-DOPA. By summing all contributions except the one from the Cl atom in Cl-DOPA, we end up with an overall lower stabilization (-0.225) as a whole compared with the same sum performed for DOPA (-0.241) whereas the inclusion of the additional contribution from Cl in the case of Cl-DOPA is sufficient to change the balance in favour of a larger global stabilization observed in the case of Cl-DOPA (ΔE of -0.269 as a whole). This observation is consistent with the higher voltage of Cl-DOPA compared to the one of DOPA, which originates from the withdrawing effect of Cl in the case of Cl-DOPA. The same conclusion holds true for the comparison of these two compounds by considering now the case of Na single reduction process (global ΔE of -0.110 *vs.* 0.004 for DOPA and Cl-DOPA, respectively). In that case, for both compounds a much lower global ΔE extent than for the single Li-reduction is observed, thus accounting for the global lower redox voltages observed in the case of Na-single reduction compared to the Li-single one. On the other hand, while Cl-DOPA is still exhibiting higher redox voltage than DOPA, in agreement with the above-mentioned considerations on ΔE, the main driving force of this effect is now linked in that case to a more efficient 6MR stabilization for Cl-DOPA. For all two-electron processes involving either Li^+, Na^+ or Mg^{2+}, a more stabilizing global ΔE is again observed for Cl-DOPA compared to DOPA (*i.e.* -0.499 *vs.* -0.443 ; -0.166 *vs.* -+0.228 ; -0.404 *vs.* -0.240 for Cl-DOPA vs. DOPA in Li-, Na-, and Mg-electrochemistry, respectively), consistently with the higher redox-voltage of this compound in all these situations. Once more, focusing on the ΔE sum excluding the Cl contribution for Cl-DOPA sheds light on the role of the Cl atom on the redox potential: for the Li-double reduction, its large extent (-0.109) is responsible for the larger voltage compared to DOPA since otherwise the ranking situation among the two compounds would be the reverse. Nevertheless, for the Mg-two electron process, the stabilization provided by this atom is roughly half this value (-0.057) and the ΔE sum excluding this contribution would be sufficient to generate a higher voltage than for DOPA while for the Na-double reduction the almost zero contribution (-0.001) indicates that in this case the Cl atom does not affect the redox potential value (the DOPA compound being in that case characterized by both a lower stabilization and a larger destabilization of the O1).

Similarly, it is important to compare the cases of *L*-DOPA and CQ, which are characterized by pieces of the FG being comparable, while having distinctions (the FG corresponding to CH_2-$CH(NH_2)$-COOH and CH=CH-COOH for *L*-DOPA and CQ, respectively). The redox voltages of the two *o*-quinones exhibiting much less differentiation for Li-single reduction than the two above mentioned compounds is linked to very similar energy stabilization provided by both the 6MR (-0.303 for CQ *vs.* -0.298 for *L*-DOPA), the FG (-0.049 for CQ *vs.* -0.050 for *L*-DOPA), and O atoms of the redox centres (*i.e.* O1) (0.110 for CQ *vs.* 0.096 for *L*-DOPA), the very slightly difference global stabilization observed for CQ (-0.252 compared to -0.242 for *L*-DOPA) being consistent with the electrochemical features, exhibiting only slightly redox voltage in the case of CQ. For Na-single reduction for which a much higher redox voltage differentiation between the two compounds is observed, the global ΔE values (-0.036 for CQ *vs.* -0.012 for *L*-DOPA) are accounting of this effect as well. A large part of this aspect can be ascribed to the FG values (0.017 for CQ *vs.* 0.031 for *L*-DOPA), which are detrimental to *L*-DOPA and thus produces a lower redox voltage of this compound. For CQ and contrary to the case of *L*-DOPA, the possibility of having electron delocalization within the FG (C=C double bond combined with the positive mesomeric effect (+M) of COOH) – which latter being furthermore devoid of electron releasing NH_2 group – is fully

View Article Online
DOI: 10.1039/D0CP02045A

supporting this quantitative interpretation. For all Li/Na/Mg two-electron processes, the CQ system is characterized by higher global ΔE sum than the ones of *L*-DOPA, consistently with the higher redox potential of CQ compared to *L*-DOPA. For the Mg-double reduction, the sum of O1 and 6MR contributions in the case of CQ is already more stabilizing than the same sum performed on *L*-DOPA but the less destabilizing ΔE value coming from the FG accentuates this phenomenon. For the Na-two electron process, the same effect occurs, with the contribution of FG being this time more destabilizing in *L*-DOPA than in CQ. In the case of the Li-double reduction, the difference in stabilization almost only originates from the (6MR + O1) ΔE value since the FG contributions are nearly identical for both compounds. Additionally, HMQ and DOPA compounds exhibit quite similar ranges of global ΔE sum, in agreement with the comparable predicted reduction potentials for both molecules, the slightly larger stabilization of HMQ in the case of the double reduction producing a slightly larger redox voltage.

4.5 Net atomic charge and electrostatic interactions evolutions

Finally, we considered the net atomic charges (in complement to metal (M) … Oxygen (O) interatomic distances involved in the considered metal-anion clusters) to account for the electrostatic interactions, which could play a part in the relative extent of redox potentials as well. While the global ΔE trends (Figure 8) consistently reproduce higher stabilization for each metal cation/reduction type, of the CQ and Cl-DOPA systems (and thus higher redox potential), an elucidation is still needed especially for higher redox voltages in the case of Mg-based systems compared to the pendant Li-ones in the case of double reduction. It is therefore important to search for an eventual global shifting effect due to electrostatic interactions, which would help to recover, for instance in the case of double reduction, the following ranking: Li<Mg for the redox potential.

Figure 9 displays the extent of the global sum of Bader's net atomic charge (Q values) for the two O1 species in the initial, intermediate and final states while Table 3 gathers a few indications on the variation in Bader's net atomic charge, Q (ΔQ values) and in Bader's electron spin populations, S (ΔS values, with S=0 for the initial state), upon single reduction or two-electron processes for Li-, Na- and Mg-based compounds. In the SI, Table SI-1 gathers the Bader net atomic charges for Li, Na, and Mg species in the intermediate and final states, which exhibit as a whole little differentiation among the various systems and almost complete ionization of the metal atoms. It is clear from Table 3 and Figure 9 that the considered reduction processes generate both a differentiation in terms of type of procedure (*i.e.* one-electron *vs.* two-electron) and as a function of the nature of electrochemistry (Li/Na/Mg). The extent of the sum of the Bader's net atomic charge (Q) of the two O1 species is largely rising in absolute value from initial to intermediate and from intermediate to final states while the distinction produced in link with the type of involved metal ion is of much less magnitude.

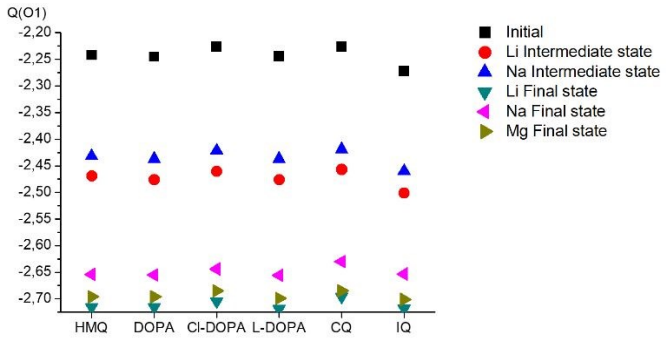

Figure 9. Representation of the global sum of Bader's net atomic charge (Q values) for the two O1 species in the initial, intermediate and final states.

View Article Online
DOI: 10.1039/D0CP02045A

Table 3. Variation in Bader's net atomic charge, Q (ΔQ values) and in Bader's electron spin populations, S (ΔS values, with S=0 for the initial state), upon one-electron (SR, single reduction) or two-electron (DR, double reduction) processes for Li-, Na- and Mg- based compounds. ΔQ(O1) and ΔS(O1) values concern the two O from the 6MR taken as a whole, while ΔQ(O2) and ΔS(O2) are related to the O from the Functional Group.

System Cation /Reduc-tion	ΔQ (O1)	ΔQ (O2)	ΔS (O1)	ΔS (O2)	ΔQ (N)	ΔQ (Cl)
HMQ						
Li/SR	-0.228	0.013	0.414	0.010	–	–
Li/DR	-0.474	0.010	–	–	–	–
Na/SR	-0.190	0.013	0.436	0.010	–	–
Na/DR	-0.412	0.008	–	–	–	–
Mg/DR	-0.454	0.004	–	–	–	–
DOPA						
Li/SR	-0.231	-0.004	0.409	–	–	–
Li/DR	-0.472	-0.008	–	–	–	–
Na/SR	-0.192	-0.005	0.431	–	–	–
Na/DR	-0.410	-0.009	–	–	–	–
Mg/DR	-0.452	-0.009	–	–	–	–
Cl-DOPA						
Li/SR	-0.234	–	0.408	–	-0.004	-0.056
Li/DR	-0.479	–	–	–	-0.009	-0.122
Na/SR	-0.196	–	0.429	–	-0.004	-0.067
Na/DR	-0.418	–	–	–	-0.009	-0.134
Mg/DR	-0.459	–	–	–	-0.008	-0.116
***L*-DOPA**						
Li/SR	-0.233	-0.003	0.408	0.001	-0.004	–
Li/DR	-0.476	-0.007	–	–	-0.007	–
Na/SR	-0.194	-0.003	0.429	0.001	-0.004	–
Na/DR	-0.413	-0.008	–	–	-0.008	–
Mg/DR	-0.456	-0.006	–	–	-0.008	–
CQ						
Li/SR	-0.231	-0.012	0.405	0.017	–	–
Li/DR	-0.470	-0.030	–	–	–	–
Na/SR	-0.193	-0.014	0.424	0.017	–	–
Na/DR	-0.404	-0.036	–	–	–	–
Mg/DR	-0.459	-0.025	–	–	–	–
IQ						
Li/SR	-0.229	–	–	–	-0.016	–
Li/DR	-0.446	–	–	–	-0.028	–
Na/SR	-0.188	–	–	–	-0.016	–
Na/DR	-0.382	–	–	–	-0.029	–
Mg/DR	-0.429	–	–	–	-0.028	–

Figure 9 highlights another important feature: for each compound, the sum of the two O1 Bader's net atomic charge species is always more negative when passing from Na to Li whatever the type of reduction process. Combined with much longer M…O interatomic distances (lying in between 2.11 and 2.19 Å) involved in the case of Na-doped systems (Figure SI-1), this induces much less stabilization originating from electrostatic interactions in the case of Na-based systems compared to Li-ones. This effect thus enhances the already existing trend of lower stabilization of Na-based systems compared to the Li-ones, as already exemplified from ΔE considerations (Figure 8).

Quite similar values of the global net atomic charge of O1 species are found after the double reduction in the case of Li- and Mg-based systems. Accordingly, since all M…O interatomic distances are around 1.91 Å for the final state of Mg^{2+}-systems and roughly in between 1.75 and 1.84 Å for final Li^{+}-systems involving a bidentate along with a further single Li^{+}-O interaction, we can conclude that electrostatic interactions will be more efficient for the sole bidentate interaction involving Mg^{2+} than the corresponding one with Li^{+}. Indeed, quite similar distances are in that case involved for a divalent species against monovalent cation for the $(Li^{+})_2$-complex, this latter being furthermore a configuration leading to non-negligible unfavourable Li^{+}-Li^{+} electrostatic repulsions in the case of the

View Article Online
DOI: 10.1039/D0CP02045A

monovalent double reduced system. These effects take part to the noticeable differentiation in terms of redox potentials between Li^+ and Mg^{2+} based systems, by globally succeeding in shifting all these latter metal-anion clusters towards higher voltages than the one exhibited for the first kind of these entities.

5. Concluding remarks

Prior to any experiment, a theoretical model was built-up to rationalize molecular electrochemical features of organic compounds. A comprehensive methodology encompassing accurate electronic structure analysis as well as identification of very specific features driving either the redox potential trends or the preferential alkaline or alkaline-earth cation location in the vicinity of redox centres was set up.

Such procedure enables to probe the redox activity capabilities of various *o*-quinones which could be potentially derived very easily from biomass-extractible catechol compounds (HMC, DA, DHI, Cl-DA, L-DA, CA) and serve as potential positive organic electrodes. Thanks to the various gathered structure-activity relationships, some guidelines on the prominent factors able to elaborate the ranking of compounds is accessible before complete knowledge of corresponding crystalline phases. In particular, ESP maps were found to be quite powerful to predict in most of cases the correct positioning of the metal-ion in the neighbourhood of the reduced molecule upon either one- or two-reduction process. Regarding the redox voltage rationalization, effects of relative stabilization accompanying the redox process were first probed through the delocalization indices HOMA and FLU of the 6MR, which are in fact insufficient to fully account for the electrochemical features ranking. To complete these initial observations, the molecular energy of each form involved during the electrochemical process was partitioned through the QTAIM methodology in suitable atomic and atomic group contributions. Such procedure reveals to be of great usefulness by allowing to identify the prevailing effect of the 6MR stabilization upon the reduction process with respect to other contributions despite its failure to account for the differentiation of systems in terms of redox potentials. Concomitantly, the incidence of other groups playing a role in the global redox potential ranking of molecules was also evidenced, therefore demonstrating that such Bader's energy partitioning can serve as a pivotal tool for the search of optimal compounds in the required electrochemical window according to the targeted application. Indeed, the ΔE trends combined with electrostatic interactions are suitable to rationalize many aspects concerning the predicted electrochemical features.

With respect to the substituent effect, one of the main information gained in the present study is the following: whatever the reduction type (single or double) and the nature of electrochemistry (Li/Na/Mg), CQ and Cl-DOPA emerge as the best candidates (from a molecular point of view) for positive electrodes, with higher redox potentials than other studied compounds. Moreover, other key findings were evidenced, which can be critical for designing new compounds with tailored redox properties: (1) single reduction involves higher redox potential values than the double one owing at least in large part to higher extent of stabilization of the *o*-quinone 6MR ; (2) an upshift/downshift of the redox potential by switching from Li to Mg/Na electrochemistry is revealed whatever the type of electrochemical process (either single (only between Li and Na in that case) or double), such shift involving an almost constant magnitude only in the particular case of the comparison between Li and Na for a double reduction; (3) different

Journal Name ARTICLE

View Article Online
DOI: 10.1039/D0CP02045A

substituent effects are observed on the single/double reduction potentials and as a function of type of electrochemistry (Li/Na/Mg), with significantly larger FG contribution on the two-electron redox potentials, compared to the one-electron process in the case of Li-electrochemistry ; (4) the ΔE partitioning is able to decipher the effects of combined functionalization or tuning of substituent effect (*e.g.* comparison of Cl-DOPA/DOPA on one hand and *L*-DOPA/CQ on the other hand). As a whole, this complete approach, taking advantage of electronic structure scrutinization in many ways, allows for drawing very clear pictures of the effects driving the redox processes in the selected set of selected *o*-quinones. Beyond this investigation focused on electrode materials for next-generation organic batteries (including metal-ion tuning and multivalent technologies), applying such methodology is able to pave the road towards novel inventive chemical approaches in even broader fields of research.

Conflicts of interest

There are no conflicts to declare.

Acknowledgements

This work was granted access to the HPC resources of IDRIS under the allocation 20*19-[*A0070806732*]* made by GENCI and was also performed by using the facilities and computing time of the supercomputer centre MCIA of the University of Bordeaux and Pays de l'Adour.

Keywords: Mono- (Li^+, Na^+) and divalent (Mg^{2+}) battery materials, Organic electrodes, *Ortho*-quinones, Redox properties, Computational studies, Delocalization indices and energy partitioning

Notes and references

View Article Online
DOI: 10.1039/D0CP02045A

1 T. B. Schon, B. T. Mc Allister, P. F. Li and D. S. Seferos, *Chem. Soc. Rev.*, 2016, **45**, 6345–6404.

2 J. Xie and Q. Zhang, *J. Mater. Chem. A*, 2016, **4**, 7091–7106.
3 R. H. Thomson, Naturally Occurring Quinones IV Recent Advances, 4th ed. London: Blackie; 1997.
4 S. K. Carter, S. T. Crooke and C. Mitomycin, Current Status and New Developments, New York Academic Press, 1979.
5 W. A. Remers and R. T. Dorr, in Alkaloids: Chemical and Biological Perspectives, S.W. Pelletier editor, New York Wiley, 1988, pp. 1–74.
6 R. W. Franck and M. Tomasz, in Chemistry of Antitumor Agents, D.E.V. Wilman Editor, Glasgow Blackie and Son Ltd., 1990, pp. 379–393.
7 S. J. Danishefsky and J. M. Schkeryantz, *Synlett.*, 1995, pp.475–490.
8 Y. J. Kim, W. Wu, S. E. Chun, J. F. Whitacre and C. J. Bettinger, *Adv. Mater.*, 2014, **26**, 6572–6579.
9 A. Jouhara, N. Dupré, A. C. Gaillot, D. Guyomard, F. Dolhem and P. Poizot, *Nat. Commun.*, 2018, **9**, 4401, 1–11.
10 A. Beheshti, P. Norouzi, M. R. Ganjali, *Int. J. Electrochem. Sci.*, 2012, **7**, 4811.
11 C. Frayret, D. Tomerini, C. Gatti, Y. Danten, M. Becuwe, F. Dolhem and P. Poizot, *Adv. Sci. Tech.*, 2014, **93**, 146-151.
12 D. Tomerini, C. Gatti and C. Frayret, *Phys. Chem. Chem. Phys.*, 2015, **17**, 8604-8608.
13 D. Tomerini, C. Gatti and C. Frayret, *Phys. Chem. Chem. Phys.*, 2016, **18**, 2442-2460.

14 D. Tomerini, O. Politano, C. Gatti and C. Frayret, *Phys. Chem. Chem. Phys.*, 2016, **18**, 26651-26660.
15 S. Er, C. Suh, M. P. Marshak and A. Aspuru-Guzik, *Chem. Sci.*, 2015, **6**, 885–893.

16 J. E. Bachman, L. A. Curtiss, and R. S. Assary, *J. Phys. Chem. A*, 2014, **118**, 8852−8860.

17 K. C. Kim, T. Liu, S. Woo Lee, and Seung Soon Jang, *J. Am. Chem. Soc.*, 2016, **138**, 2374−2382.
18 Z. Niu, H. Wu, Y. Lu, S. Xiong, X. Zhu, Y. Zhao and X. Zhang, *RSC Adv.*, 2019, **9**, 5164–5173.
19 L. Miao, L. Liu, Z. Shang, Y. Li, Y. Lu, F. Cheng, J. Chen, *Phys. Chem. Chem. Phys.,* 2018, 20, 13478–13484.
20 *J. Phys. Chem. C*, 2012, **116**, 3793−3801.
21 M. T. Huynh, C. W. Anson, A. C. Cavell, S. S. Stahl, S. Hammes-Schiffer, *J. Am. Chem. Soc.*, 2016, **138**, 49, 15903-15910.
22 C. Guo, Weihua Wang, W. Feng and P. Li, *RSC Adv.*, 2017, **7**, 12775–12782.
23 N. Macías-Ruvalcaba, G. Cuevas, I. González, M. Aguilar-Martınez, *J. Org. Chem.*, 2002, **67**, 3673–3681.
24 M. Gómez, F.J. González, I. González, *J. Electrochem. Soc.* 2003, **150**, E527.
25 M. Namazian, H. A. Almodarresieh, M. R. Noorbala, H. R. Zare, *Chem. Phys. Lett.* 2004, **396**, 424–428.
26 D. Moraleda, D. El Abed, H. Pellissier, M. Santelli, *J. Mol. Struct.* (*THEOCHEM*) 2006, **760**, 111.
27 J. Conradie, *J. Phys: Conf. Ser.* 2015, **633**, 012045, 1–6.
28 S. E. Burkhardt, M. A. Lowe, S. Conte, W. Zhou, H. Qian, G. G. Rodríguez-Calero, J. Gao, Richard G. Hennig and H. D. Abruña, Energy Environ. Sci., 2012, 5, 7176–7187.
29 Y. Ding, Y. Li, G. Yu, *Chem 1*, **November 10**, 2016, 790-801.
30 M. T. Huynh, C. W. Anson, A. C. Cavell, S. S. Stahl, and S. Hammes-Schiffer, *J. Am. Chem. Soc.* 2016, **138**, 49, 15903–15910.
31 C. Frontana, A. Vázquez-Mayagoitia, J. G. Rubicelia Vargas, and I. González, *J. Phys. Chem. A* 2006, **110**, 9411-9419.

32 A. Beheshti, P. Norouzi, M. R. Ganjali, *Int. J. Electrochem. Sci.,* 7 (2012) 4811 – 4821.
33 Y. L. Jong, J. K. Geum, K. C. Jin, A. C. Young, H. J. Na, P. H. Park, C.i Hyukjae and S.-H. Kim, *Front. Pharmacol.*, **2018**, *9*, 726, 1–12.
34 P. Luliński and D. Maciejewska, *J. Sep. Sci.*, **2012**, *35*, 1050–1057.
35 P. Zhao, Z. Lu, Michael R. Strand and H. Jiang, *Insect Biochem. Mol.*, **2011**, *41*, 645-652.
36 L. García-Fernández, J. Cui, C. Serrano, Z. Shafiq, R. A. Gropeanu, V. San Miguel, J. I. Ramos, M. Wang, G. K. Auernhammer and S. Ritz, *Adv. Mater.* **2013**, *25*, 529–533.
37 K. B. Ramya and S. S. Thaakur, *Anc. Sci. Life*, **2007**, *27*, 50–55.
38 L. Misra and H.L. Wagner, *Indian J. Biochem. Biophys.*, **2007**, *44*, 56-60.
39 S. A. O. Santos, C. S. R. Freire, M. R. M. Domingues, A. J. D. Silvestre and N. C. Pascoal, *J. Agric. Food Chem.* **2011**, *59*, 9386–9393.
40 C. S. Khoo, S. Sullivan, M. Kazem, F. Lamin, S. Sing, M. Nang, H. Suresh; S. Lee, International Scholarly Research Notices (2014) Retrieved 2019-01-22.
41 M. I. Choudhary, N. Naheed, A. Abbaskhan, S. G. Musharraf, H. Siddiqui, A. U. Rahman, *Phytochemistry*, ***2008**, 69, 1018–1023.*
42 Y. S. Lee, Y. H. Kang, J. Y. Jung, S. Lee, K. Ohuchi, K. H. Shin, I.J. Kang, J. H. Y. Park, H. K. Shin, S. Soon, *Biol. Pharm. Bull.*, ***2008**, 31, 1968–1972.*
43 H. Pulikkalpura, R. Kurup, P. J. Mathew, S. Baby, *Sci. Rep.*, *5*, 11078.
44 Y. J. Kim, W. Wu, S.-E. Chun, J. F. Whitacre, C. J. Bettinger, *Adv. Mater.*, 2014, **26**, 6572–6579.
45 M. J. Frisch, G. W. Trucks, H. B. Schlegel, G. E. Scuseria, M. A. Robb, J. R. Cheeseman, G. Scalmani, V. Barone, B. Mennucci, G. A. Petersson, H. Nakatsuji, M. Caricato, X. Li, H. P. Hratchian, A. F. Izmaylov, J. Bloino, G. Zheng, J. L. Sonnenberg, M. Hada, M. Ehara, K. Toyota, R. Fukuda, J. Hasegawa, M. Ishida, T. Nakajima, Y. Honda, O. Kitao, H. Nakai, T. Vreven, J. A. Montgomery, Jr., J. E. Peralta, F. Ogliaro, M. Bearpark, J. J. Heyd, E. Brothers, K. N. Kudin, V. N. Staroverov, R. Kobayashi, J. Normand, K. Raghavachari, A. Rendell, J. C. Burant, S. S. Iyengar, J. Tomasi, M. Cossi, N. Rega, J. M. Millam, M. Klene, J. E. Knox, J. B. Cross, V. Bakken, C. Adamo, J. Jaramillo, R. Gomperts, R. E. Stratmann,

Journal Name ARTICLE

View Article Online
DOI: 10.1039/D0CP02045A

O. Yazyev, A. J. Austin, R. Cammi, C. Pomelli, J. W. Ochterski, R. L. Martin, K. Morokuma, V. G. Zakrzewski, G. A. Voth, P. Salvador, J. J. Dannenberg, S. Dapprich, A. D. Daniels, O. Farkas, J. B. Foresman, J. V. Ortiz, J. Cioslowski and D. J. Fox, Gaussian, Inc., Gaussian 09, Revision D.01 2009.
46 A. V. Marenich, C. J. Cramer, and D. G. Truhlar, *J. Phys. Chem. B*, 2009, **113**, 6378–6396.
47 A. E. Lakraychi, F. Dolhem, F. Djedaïni-Pilard, A. Thiam, C. Frayret, M. Bécuwe, *J. Power Sources*, 2017, **359**, 198–204.

48 R. F. W. Bader, *Atoms in Molecules: A Quantum Theory,* Clarendon Press, Oxford, 1994.
49 J. Kruszewski, T. M. Krygowski, *Tetrahedron Lett.*, 1972, **36**, 3839-3842.
50 T. M. Krygowski, *J. Chem. Inf. Comput. Sci.*, 1993, **33**, 70–78.
51 T. M. Krygowski, M. Cyrański, *Tetrahedron*, 1996, **52**, 10255–10264.
52 E. Matito, M. Duran and M. Solà, *J. Chem. Phys.*, 2005, **122**, 014109-1–014109-8.

53 V. Tognetti and L. Joubert*, ChemPhysChem,* 2017*,* **18***,* 2675–2687.
54 C. Gatti, SF-ESI codes, private communication.

55 T. D. Chung, D. Choi, S. K. Kang, S. K. Lee, S. K. Chang, and H. Kim, *J. Electroanal. Chem.*, **1995**, *396*, 431–439.

56 N. Patil, A. Mavrandonakis, C. Jérôme, C. Detrembleur, J. Palma, and R. Marcilla, *ACS Appl. Energy Mater.* **2019**, *2*, 3035−3041.